ACS APPLIED MATERIALS & INTERFACES

Research Article

www.acsami.org

Interfacial Stress Transfer in Graphene Oxide Nanocomposites

Zheling Li, Robert J. Young,* and Ian A. Kinloch

School of Materials, University of Manchester, Oxford Road, Manchester M13 9PL, United Kingdom

Supporting Information

ABSTRACT: Raman spectroscopy has been used for the first time to monitor interfacial stress transfer in poly(vinyl alcohol) nanocomposites reinforced with graphene oxide (GO). The graphene oxide nanocomposites were prepared by a simple mixing method and casting from aqueous solution. They were characterized using scanning electron microscopy, X-ray diffraction, and polarized Raman spectroscopy and their mechanical properties determined by tensile testing and dynamic mechanical thermal analysis. It was found that GO was fully exfoliated during the nanocomposite preparation process and that the GO nanoplatelets tended align in the plane of the films. The stiffness and yield stress of the nanocomposites were found to increase with GO loading but the extension to failure decreased. It was shown that the Raman D band at ~1335 cm^{-1} downshifted as the nanocomposites were strained as a result of the interfacial stress transfer between the polymer matrix and GO reinforcement. From knowledge of the Grüneisen parameter for graphene, it was possible to estimate the effective Young's modulus of the GO from the Raman D band shift rate per unit strain to be of the order of 120 GPa. A similar value of effective modulus was found from the tensile mechanical data using the "rule of mixtures" that decreased with GO loading. The accepted value of Young's modulus for GO is in excess of 200 GPa and it is suggested that the lower effective Young's modulus values determined may be due to a combination of finite flake dimensions, waviness and wrinkles, aggregation, and misalignment of the GO flakes.

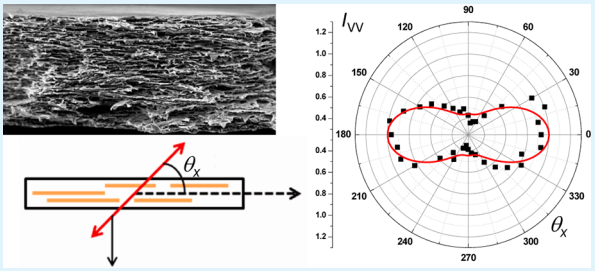

KEYWORDS: *graphene-oxide, Raman spectroscopy, nanocomposite, mechanics, reinforcement efficiency*

INTRODUCTION

Since it was first successfully exfoliated in 2004,[1] graphene has attracted a rapid increase in attention for applications in a variety of fields, including graphene-based actuators[2,3] and graphene-reinforced nanocomposites.[4−6] Its derivative graphene oxide (GO) is playing an increasingly important role, because of its excellent properties and the ability to produce it in large quantities at relatively low cost.[7] The detailed structure of GO is a matter of considerable debate[8−10] but it is known that it contains different oxygen functional groups such as epoxide, hydroxyl, and carbonyl groups,[5] which enable hydrophilic graphene oxide to be dispersed homogeneously in water and water-soluble polymers, such as poly(vinyl alcohol) (PVA).[11−14] There is also the possibility of forming bonds between the GO layers and PVA molecules, which unlike graphene, has the potential to increase the interfacial adhesion in the nanocomposites significantly.

Although the interface between the reinforcement and matrix may have been strengthened, the mechanical properties of GO are thought to be inferior to those of graphene.[15] According to a recent comparison,[16] the mechanical properties of GO-based PVA nanocomposites are unexpectedly not as good as those of an equivalent graphene-based nanocomposite. It appears therefore that a balance needs to be struck between the inherent mechanical properties of the reinforcement and the strength of the interface between the polymer and the graphene-based reinforcement.

Raman spectroscopy has been used widely to follow stress transfer between the matrix and reinforcement in a wide range of polymer-based composites. In general, the shift in the Raman band rate is proportional to the stress or strain in the reinforcement due to changes in bond length.[17] As the bond elongates, which on the macroscale is equivalent to tensile strain, the Raman wavenumber generally undergoes a red-shift that reverses on unloading.[18] In carbon-based composites, both the G band and 2D band[19] have been used to follow the strain in the reinforcement (including carbon fibres,[20] carbon nanotubes[21] and exfoliated graphene[22] etc.), thus providing an insight into the deformation micromechanics. In the case of GO, however, unlike graphene, the 2D band is very weak,[23] and the G band is broad[24] with a weaker D′ band incorporated in it. This makes it difficult to use the 2D and G Raman to monitor deformation in GO-based nanocomposites.

In order to solve these difficulties in using Raman spectroscopy to follow the deformation of GO-based nanocomposites, an investigation has been undertaken upon using the shift of the Raman D band to follow interfacial stress transfer between the PVA and GO reinforcement. It will be shown that significant shifts of the D band are found during the deformation of GO/PVA nanocomposites that enable the mechanics of deformation to be studied in detail.

Received: November 5, 2012
Accepted: December 21, 2012
Published: December 21, 2012

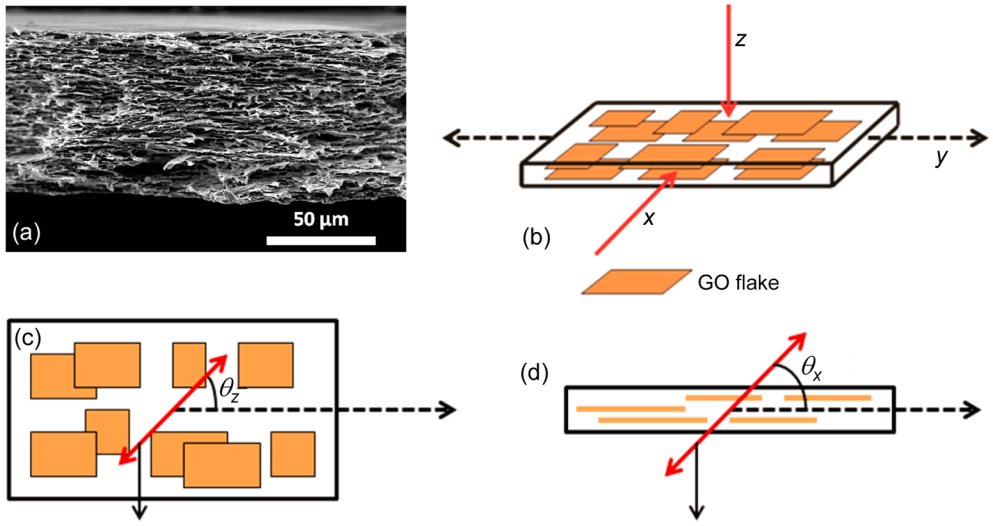

Figure 1. (a) SEM micrograph showing the layered microstructure of the 5 wt % GO/PVA nanocomposite. (b) Schematic illustration of the geometry of the Raman spectroscopic analysis of the GO/PVA nanocomposites films with (c) the laser beam parallel to *z*, and (d) the laser beam parallel to *x*. (The double headed arrows in c and d indicate the axes of laser polarization).

EXPERIMENTAL SECTION

Materials. The PVA ($M_w \approx$ 89 000−98 000, 99+% hydrolyzed) was purchased from Sigma Aldrich and used as received. The graphite (Grade 2369) was supplied by Graphexel Ltd. All other reagents were of analytical grade and used without further purification.

Graphene Oxide Preparation. The GO was prepared using the modified Hummers method.[25,26] Briefly, 3 g of graphite was added to 70 mL of concentrated sulfuric acid while stirring at room temperature. The mixture system was then cooled to 0 °C when 1.5 g sodium nitrate was added. While stirring, 9 g of potassium permanganate was added slowly, to avoid a rapid temperature rise. The mixture was then placed into a 40 °C water bath for 0.5 h, followed by the addition of 140 mL of water and it was stirred for another 15 min. An additional 20 mL of 6% w/v H_2O_2 and 500 mL of water were added subsequently, after which the color of the mixture turned from brown to yellow. The mixture was then repeatedly washed with 250 mL of 1:10 HCl aqueous solution and centrifuged 3 times. Following this, the mixture was repeatedly washed with water and centrifuged until the pH was approximately 7. Finally, the GO was dispersed in water to make an aqueous suspension for later use.

GO/PVA Nanocomposites Preparation. The PVA powder was dissolved in water at 90 °C to give a 10 wt % PVA aqueous solution. The GO suspension and PVA solution were then mixed to form a series of dispersions with GO concentrations of 1, 2, 3, and 5 wt %. Neat PVA solution was used as a comparison. These solutions were placed into a 120 W sonication bath for 30 min to obtain homogeneous dispersions. They were then allowed to stand overnight to fully remove any bubbles. For mechanical testing, the dispersions were cast into glass Petri dishes at room temperature for film formation. For the Raman deformation studies, the dispersions were cast onto PMMA beams. In both cases, the nanocomposites formed were allowed to dry under ambient conditions for 1 week to ensure complete evaporation of the aqueous component.

Scanning Electron Microscopy. SEM images were obtained using EVO60 VPSEM (Zeiss). Samples were fractured by hand at room temperature and fixed vertically with the fracture surface toward the electron gun. The surfaces were coated with gold before analysis. Fracture surfaces of the specimens following failure during mechanical testing were also examined using SEM.

X-ray Diffraction. X-ray diffraction was carried out on the nanocomposite films using an X'Pert DY609 X-ray diffractometer (Philips) with a Cu Kα radiation source (λ = 1.542 Å).

Mechanical Testing. The tensile properties of the neat PVA and GO/PVA nanocomposites with different loadings were evaluated using an Instron-1122 universal testing machine. The film samples were cut into dumbbell shape with a gauge length of 15 mm, a width of 3.96 mm, and a thickness of around 0.075 mm. Before testing the samples were left in a climate-controlled laboratory for 24 h at a temperature of 23.0 ± 0.1 °C and a relative humidity of 50 ± 5%. The specimens were deformed at a loading rate of 1 mm/min and between 4 and 6 specimens of each of the nanocomposites compositions were tested.

The dynamic mechanical properties were also evaluated using a DMA Q800 (TA Instruments). Specimens with a thickness of around 0.075 mm were heated from −10 to 120 °C at a rate of 3 °C/min and deformed using a frequency of 1 Hz and a static force of 0.005 N. Data were averaged from 2 to 3 specimens for each nanocomposite composition.

The GO loading was converted from mass fraction w_g (wt%) to volume fraction v_g (vol%) using the rule of mixtures.[14]

$$v = \frac{w\rho_p}{w\rho_p + (1-w)\rho_g} \quad (5)$$

Here, ρ_p and ρ_g represent the density of PVA and GO, which were 1.3 and 2.2 g/cm^{-3}, respectively.[4,12,27] As a result, the mass fractions of 1, 2, 3, and 5 wt % GO/PVA are equivalent to volume fractions of 0.6, 1.2, 1.8, and 3.0 vol%, respectively.

Raman Spectroscopy. Raman spectroscopy was conducted using a Renishaw 2000 Raman spectrometer system with a HeNe laser (633 nm excitation). The orientation of the GO in the nanocomposite was determined using a rotation stage on the spectrometer optical microscope and different combinations of parallel and perpendicular polarization of the incident and scattered light. In situ Raman deformation analysis of the nanocomposites was conducted using the same spectrometer. The PMMA beams with GO/PVA films on their surface were deformed in a four-point bending rig placed on the Raman microscope stage. A resistance strain gauge was bonded to the specimen surface using cyanoacrylate adhesive to measure the surface strain. The beam was deformed stepwise and Raman spectra were collected from the central area of nanocomposite at each strain level. The polarization of the incident laser parallel to the tensile direction, and the laser beam focused to a spot of around 2 μm diameter.[28]

RESULT AND DISCUSSION

Microstructure of the GO and GO/PVA Films. The microstructure of the GO/PVA nanocomposites films with different GO loadings was examined using a combination of X-ray diffraction (XRD), scanning electron microscopy (SEM)

dx.doi.org/10.1021/am302581e | ACS Appl. Mater. Interfaces 2013, 5, 456−463

and polarized Raman spectroscopy. The lateral dimensions of the GO flakes were found by SEM to be up to ~10 μm (see the Supporting Information). XRD patterns for the GO and all the nanocomposite compositions are also shown in the Supporting Information. The characteristic XRD diffraction peak seen in the pure GO at 2θ = 10.5°, corresponding to a *d*-spacing of 0.84 nm between GO flakes, is not present in the nanocomposites indicating the GO flakes was fully exfoliated during the composite preparation process.[29] The XRD patterns of all of the GO/PVA nanocomposites films are similar to those of neat PVA sample with a peak at 2θ = 19.6°. No changes of this PVA peak in the nanocomposites (neither broadening nor shifting) were observed, indicating the degree of crystallinity and size of PVA crystals was not changed significantly by the incorporation of the GO.[30]

Figure 1a shows a scanning electron micrograph of a room temperature fracture surface of a PVA nanocomposite film containing 5 wt % GO in which a layered structure can be clearly seen. Fracture surfaces of samples containing all loadings studied, from 1 to 5 wt % showed similar microstructures and micrographs are given in the Supporting Information. Polarized Raman spectroscopy was used to quantify the orientation of the GO in the nanocomposites and Figure 1b shows the geometry of the specimen used for this analysis. The direction of application of the tensile stress is defined as the *y*-axis and direction perpendicular to the plane of the film is defined as the *z*-axis. The *x*-axis is the defined as the direction in the plane of the film perpendicular to the *y*- and *z*-axes. Panels c and d in Figure 1 show the definition of the angles θ_z and θ_x, respectively, through which the specimens were rotated relative to the *y*-axis (the straining direction) in order to quantify the orientation of the GO flakes.

Raman spectra were obtained from the middle of the nanocomposite films on the PMMA beams and a typical Raman spectrum of the 1 wt % GO/PVA nanocomposite is shown in Figure 2. Spectra are also given for neat PVA and neat GO

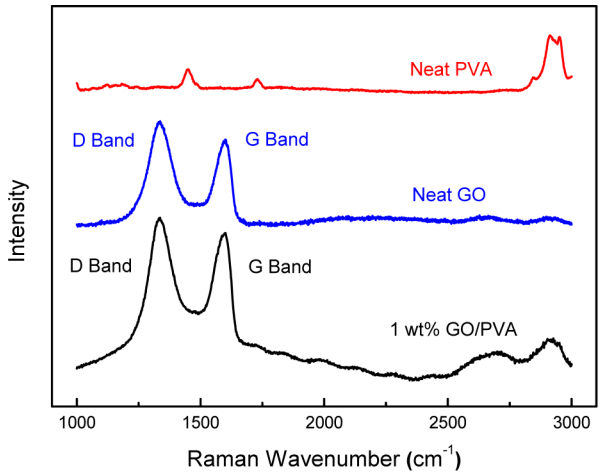

Figure 2. Raman spectrum of neat PVA, neat GO, and a 1 wt % GO/PVA nanocomposite.

powder. It can be seen that although the loading of the GO in the nanocomposite is only 1 wt % (0.6 vol%), the Raman bands of the GO dominate the spectrum for the nanocomposite.

The G band around 1600 cm^{-1} corresponds to the E_{2g} phonon at the Brillouin zone (BZ) center (Γ point).[31] The D band, which has a peak position at around 1335 cm^{-1}, is usually assigned to the K point phonons of A_{1g} symmetry, and is associated with the presence of defects.[32] The spectra of the GO and the nanocomposite are similar to those reported in the literature.[33] They are quite different, however, from the spectrum of pristine graphene,[34] which has one sharp G band and no D band. In addition, pristine graphene has a 2D (or G′) band that is absent in GO. The broad G and D bands, and a D band that is of higher intensity than the G band, are thought to be due to the presence of sp^3 carbon as a result of the amorphization of the graphite during the oxidation process.[33]

Polarized Raman spectroscopy was employed to characterize the orientation of the GO flakes in the polymer matrix using a backscattering geometry and obtaining spectra with the polarized laser beam aligned either perpendicular (in the *z*-direction) or parallel (in the *x*-direction) to the surface of the specimen film as shown in Figure 1. The film was rotated relative to the specimen axes and an analyzer was used with the scattered light. Two combinations of incident and scattered polarization were employed; VV (vertical/vertical) in which directions of the incident and scattered polarization were the same and VH (vertical/horizontal) in which they were at 90° to each other. The change in the intensities of both the D and G bands with film orientation was monitored, with only the data for the stronger D band using VV polarization presented here. In all cases the ratio of the band intensities, I_D/I_G, remained constant at ~1.1 and so the behavior of the two bands was essentially identical.

The variation of the D band intensity for the 1 wt % GO/PVA nanocomposites for the two laser beam directions with the relative orientations of the incident laser polarization are shown in Figure 3. The intensities have been normalized in each case for a maximum intensity of unity.

In the case where the laser beam is parallel to the *z*-axis (i.e., perpendicular to the plane of the film) in Figure 3a it can be seen that the D band intensity remains approximately constant as the film is rotated. In contrast, when the laser beam is parallel to the *x*-axis (Figure 3b) the D band intensity is a maximum when the direction of laser polarization is parallel to the specimen edge plane and a minimum when it is perpendicular to the edge. This is consistent with the in-plane alignment of the GO layers in the GO/PVA nanocomposites seen in the SEM micrograph in Figure 1a.

The data in Figure 3 can analyzed theoretically in terms of the depolarization effect. If the GO layers are oriented randomly in-plane then the intensity of Raman scattering with the laser beam parallel to the *z*-axis should be independent of laser polarization direction as indicated by the theoretical line. For the laser beam parallel to the *x*-axis, a relationship of the form $I_D \approx \cos^4 \theta_x$ is expected for the VV configuration.[35] The best fit to the data in Figure 3b is a function of the form

$$I_D = A\cos^4 \theta_x + B \quad (1)$$

where A = 0.56 and B = 0.44, which shows that there is a high degree of order in the in-plane stacking of the GO layers in the nanocomposites film. Similar behavior is found for the G band, and it has been found before for carbon nanotube fibers that all Raman bands, including the radial breathing modes, obey a relation of this form.[36] A $\cos^4$ dependence has also been observed for the intensity of the G band in aligned functionalized multilayer graphene sheets.[37] The constant B in the equation is most likely due to the contribution to the spectrum of randomly aligned GO. The behavior described above is for the material containing 1 wt % GO. Similar

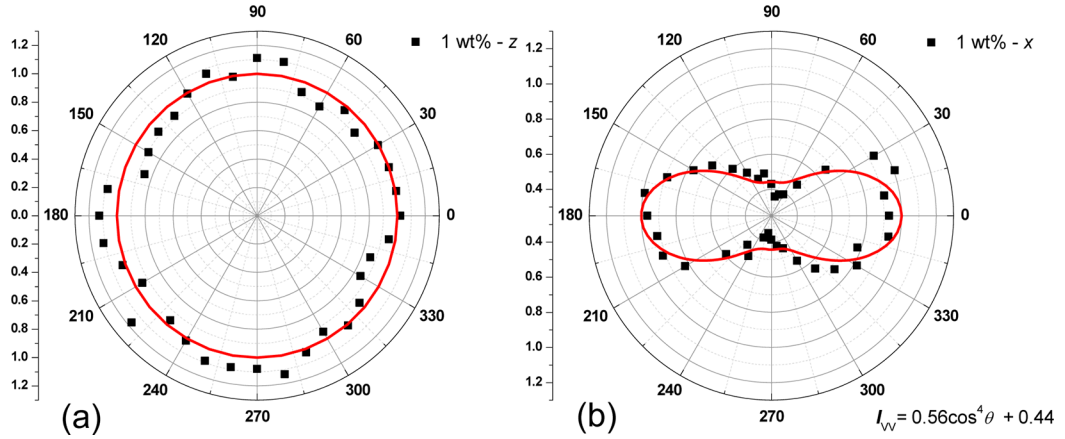

Figure 3. Polar plots of the normalized intensity of the D band using VV polarization (a) parallel to *z*, (b) parallel to *x*. The black dots represent experimental results, and the red line represents a fit to a constant value and $I_D = 0.56\cos^4 \theta_x + 0.44$ for a and b, respectively.

behavior is found for the other compositions as shown in the Supporting Information and the values of *A* and *B* determined in each case are given in Table 1.

Table 1. Storage Modulus of the GO Nanocomposites at 20 °C and Effective GO Modulus Determined Using the Rule of Mixtures; Values of the Parameters *A* and *B* from eq 1 Determined Using Polarized Raman Spectroscopy Are Also Given for Each of the Nanocomposites

materials	*A*	*B*	storage modulus (GPa)	effective GO modulus, E_{eff} (GPa)
neat PVA			4.4 ± 0.7	
1 wt % GO/PVA	0.56	0.44	5.1 ± 0.9	121 ± 21
2 wt % GO/PVA	0.53	0.47	5.7 ± 0.4	113 ± 8
3 wt % GO/PVA	0.53	0.47	6.1 ± 0.1	99 ± 2
5 wt % GO/PVA	0.34	0.66	6.5 ± 0.7	74 ± 8

The in-plane orientation of the GO sheets found in this study can be contrasted with the random orientation reported in the study of Zhao, Zhang, and Chen[14] upon a similar GO/PVA system. In the latter case, however, the GO was reduced in situ by hydrazine and the GO/PVA solution dried at 60 °C in an oven. In our case, the solution was allowed to dry under ambient conditions for a week, which appears to have enabled the GO platelets to become aligned by gravity parallel to the plane of the film.

Mechanical Properties of the GO/PVA Films. The mechanical properties of the materials were studied by tensile testing. Typical stress–strain curves for the different nanocomposites and pure PVA are shown in Figure 4a. It can be seen that the Young's modulus and yield stress of the nanocomposites increases as the GO loading increases, whereas the elongation to failure decreases. This behavior is typical of that found in previous investigations on similar systems.[14]

The variation in the storage modulus of the nanocomposites with temperature is shown in Figure 4b. It can be seen that the addition of the GO increases the storage modulus at all temperatures. Table 1 gives the values of the storage modulus for each of the compositions at 20 °C. As the GO loading increase from 0 to 5 wt %, the average storage modulus at 20 °C increases from to 4.4 to 6.5 GPa. This nearly 50% increase indicates that the dynamic mechanical properties have also been enhanced by the incorporation of GO. It is instructive to compare this behavior with that expected from theoretical considerations.

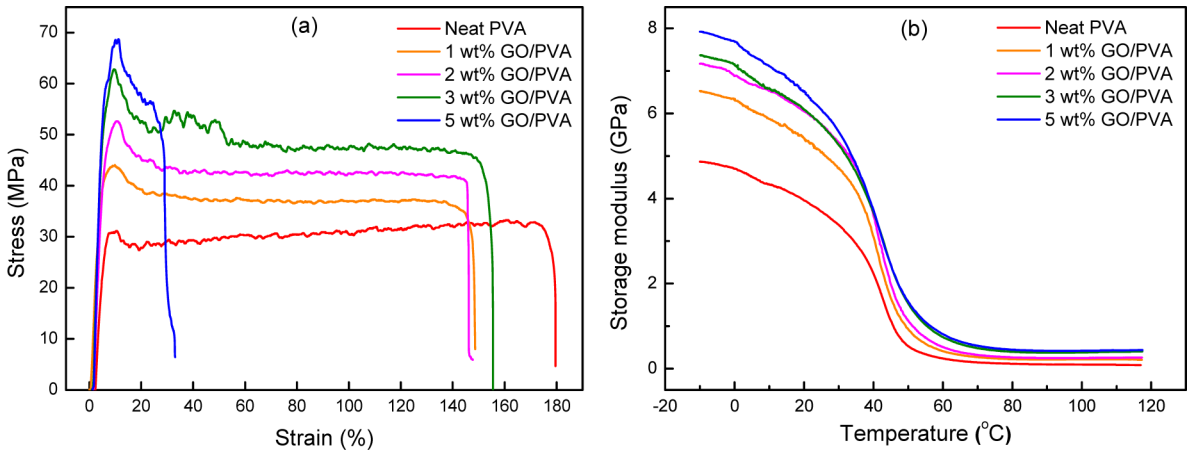

Figure 4. Mechanical properties of the neat PVA and GO/PVA nanocomposites with different GO loadings. (a) Stress–strain curves at 23 ± 1 °C and (b) storage modulus at a function of temperature.

dx.doi.org/10.1021/am302581e | *ACS Appl. Mater. Interfaces* 2013, 5, 456–463

The mechanics of the reinforcement of polymers by graphene has been reviewed recently.[6] The simplest approach to use is the rule of mixtures that provides an upper bound for the Young's modulus of a graphene-based composite E_c[38] as

$$E_c = V_g E_g + (1 - V_g)E_m \quad (2)$$

where in this case, E_g, E_m, and V_g are the effective GO modulus, matrix modulus, and volume fraction of GO, respectively. This equation would be appropriate for the situation where both the matrix and the reinforcement were subjected to uniform strain.[38] This is the situation, for example, in the case of long aligned fibres in a matrix, for which the in-plane aligned GO layers in our GO/PVA composites are a 2D analogy. On this basis, the effective modulus of the GO in the nanocomposite films can be calculated as shown in Table 1. using eq 2, it can be seen that the effective modulus of the GO falls from around 121 GPa for 1 wt % loading to 74 at 5 wt % loading.

Raman Band Shifts. It is well-established that Raman spectroscopy can be used to follow the micromechanics of deformation in a wide range of different carbon-based systems,[17−22] and the technique gives unprecedented insight into the deformation processes involved from the stress-induced Raman bands shifts. Most of the studies have been undertaken using shifts of either the G or 2D (G′) bands but there are also reports of the D band undergoing stress-induced shifts in gaphene[18] and there is one report of stress-induced shifts of the Raman G band during the deformation of impregnated GO paper.[24] Raman spectroscopy has been employed to follow deformation micromechanics in graphene-reinforced model nanocomposite,[22,39,40] but to the best of our knowledge, the technique has not yet been used for the analysis of deformation micromechanics in GO-based nanocomposites.

In this present study, Raman spectra were obtained from the GO nanocomposites, with the laser beam parallel to the z axis, during deformation and the positions of both the G and D bands were monitored as a function of strain. The G band in GO is known[24] to consist of at least two components and the overall shape of the band is asymmetric. Because of this, it was difficult to detect any well-defined band shifts for this band. Figure 5 shows the D band for the 1 wt % GO/PVA nanocomposite before and after tensile deformation to 0.4% strain and it can be seen that there is a significant strain-induced downshift of the band. Strain modifies the crystal phonons in graphene, with tensile strain resulting in mode softening.[18,19] Thus the downshift of the D band can be understood in terms of the elongation of the C−C bonds.

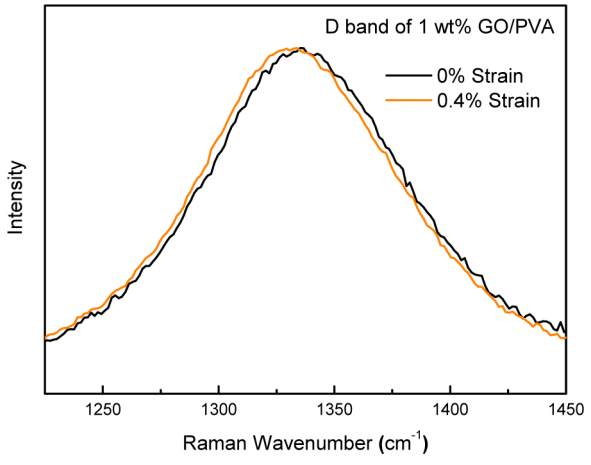

Figure 5. D band of 1 wt % GO/PVA nanocomposite before and after tensile deformation. (The intensity of D bands have been rescaled to same level).

It should be noted that shifts of these bands could also be obtained without any deformation during exposure of the nanocomposites to the Raman laser beam, especially at high power levels, presumably because of degradation of the unstable GO material in the laser beam. The data shown in this present study were all obtained at low laser power, so avoiding any problems with beam damage, and were found to be reversible and repeatable. Figure 6 shows the shift of the D band for the 5 wt % GO/PVA nanocomposite, and it can be seen that there is an approximately linear shift of the D band with strain that is reversibly upon unloading. The D band-shift behavior for all nanocomposite compositions investigated is shown in the Supporting Information. For each composition, the Raman D bands shift approximately linearly to a lower wavenumber as the strain increases, indicating good interfacial stress transfer between the GO and PVA matrix, with no obvious slippage.[22]

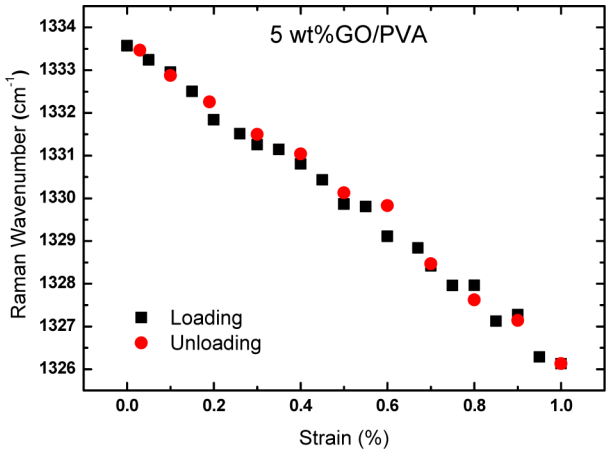

Figure 6. Shift of the D band with strain for the 5 wt % GO/PVA nanocomposite, for loading to 1% strain followed by unloading.

At least two tests were repeated for each composition and the average shift rates for 1 wt %, 2 wt %, 3 wt % and 5 wt % GO loadings are shown in Table 2 (and plotted against GO loading in the Supporting Information). It can be seen that the shift rate is approximately linear with strain and falls slightly with GO loading with an average value of around −8 cm^{-1}/% strain.

Table 2. Average Raman D Band Shift Rates for the Different Nanocomposite Compositions and Values of Effective Graphene Modulus Determined Using eq 4

samples	average D band shift rate (cm^{-1}/%)	effective GO modulus (GPa)
1 wt % GO/PVA	−8.8 ± 0.1	125 ± 2
2 wt % GO/PVA	−8.3 ± 1.4	118 ± 19
3 wt % GO/PVA	−8.3 ± 1.5	118 ± 21
5 wt % GO/PVA	−7.5 ± 0.4	106 ± 6

dx.doi.org/10.1021/am302581e | ACS Appl. Mater. Interfaces 2013, 5, 456−463

It is well-established that for carbon-based systems the Raman band shift rate for a composite can be used to estimate both the efficiency of stress transfer and the effective Young's modulus of the reinforcement, for both the 2D and G bands.[21,41] To do this for the shift in the D band detected in this present study, it is necessary to introduce the Grüneisen parameter, γ. This is a measure of how the phonon frequency is altered under a small change in the volume of the crystallographic unit cell.[42] In our case, with exfoliated GO layers, only the changes in the longitude and traverse directions during deformation need to be considered. Thus, the simplified Grüneisen parameter γ, defined as[18,43]

$$\gamma = -\frac{1}{\omega_0}\frac{\partial \omega_h}{\partial \varepsilon_h} \quad (3)$$

can be employed. The parameter $\varepsilon_h = \varepsilon_{ll}+\varepsilon_{tt}$ is the hydrostatic component of the applied strain, in which l and t refer to the directions parallel and perpendicular to the direction of applied strain, respectively. The parameters ω_0 and ω_h correspond to the phonon frequency at zero strain and the applied strain, respectively.[41] This relationship can be used to estimate the band shift as a function of applied strain for GO, from knowledge of the behavior of graphene.

In the literature,[18,43,44] it is found that the measured value of the Grüneisen parameter for graphene varies as a result of the interaction of graphene and the substrate.[31] We have therefore chosen the theoretical value for free-hanging graphene of γ = 2.7.[18,43] Thus the total shift per unit strain for the D band of graphene at 1335 cm^{-1} is calculated to be around −30 cm^{-1}/% strain, which is, of course, approximately half the value of −60 cm^{-1}/% strain found experimentally for the 2D band in graphene.[18]

It is well-established that the rate of Raman band shift per unit strain for different forms of graphitic carbon can be related to the effective Young's modulus of the material. Since graphene with a modulus of 1050 GPa[45] has a D band shift rate of −30 cm^{-1}/% strain,[43] it is possible to determine the effective modulus of the GO in the nanocomposites from the D band shift data listed in Table 2 using the following expression

$$\text{effective GO modulus} = -\frac{d\omega_D}{d\varepsilon}\frac{1050}{-30}\frac{0.34}{0.84}\ \text{GPa} \quad (4)$$

where $d\omega_D/d\varepsilon$ is the measured shift rate of the D band and the term 0.34/0.84 accounts for the higher thickness of the GO (0.84 nm, see the Supporting Information) compared with that of monolayer graphene (0.34 nm). The values of effective Young's modulus of the GO in the nanocomposite are listed in Table 2. It can be seen that the values are all in the range 106−125 GPa and similar to the effective Young's modulus determined from the storage modulus data at low GO loading.

Mechanics of Deformation. It is instructive to see how these values of Young's modulus in a composite compare with those determined directly for GO so that the effective level of reinforcement can be evaluated. Gomez-Navarro, Burghard, and Kern[46] investigated the elastic deformation of chemically reduced GO monolayers using an AFM indentation technique on a suspended film of material similar to that employed in an earlier study of exfoliated graphene.[45] GO single layers of up to 1 μm^2 in size were suspended over a trench in a SiO_2/Si wafer and force-displacement curves were obtained as the AFM tip was pushed into the film. A Young's modulus of 250 ± 150 GPa was determined, although considerable scatter was obtained in their data. They also found that GO sheets with three or more layers appeared to have a Young's modulus that was an order of magnitude lower. Suk et al.[15] undertook a similar study of the AFM indentation of GO that had not been reduced and measured a Young's modulus of 208 ± 23 GPa when they assumed an effective thickness of 0.7 nm for the GO.

A theoretical study was undertaken by Paci, Belytschko, and Schatz[47] to compare the stress−strain behavior of graphene and graphene oxide containing both epoxide and hydroxyl groups and they predicted a modulus of >1000 GPa for the pristine graphene. They simulated the structural modification to form GO and found that it led to a prediction of it having a modulus of only 750 GPa, for a sheet with the same thickness as a graphene monolayer (∼0.34 nm). In our study, the thickness of the GO as determined by X-ray diffraction was 0.84 nm which is almost 2.5 times than that of monolayer graphene (0.34 nm). This will lead to a further reduction in the effective modulus of GO from 750 GPa down to 300 GPa, which is still higher than, but closer to, the measured values.[46]

Although it is clear that in the specimens studied there is a preferred orientation of the GO in the planes of the nanocomposite films, Figure 3b shows that the alignment is by no means perfect. It can be assumed that the GO/PVA composite effectively contains two GO components as detected by polarized Raman spectroscopy, one of which is perfectly aligned and so has a D band intensity that varies as $\cos^4\theta_x$ and another component of randomly oriented GO which has a D band intensity independent of θ_x. The parameters A and B in eq 1 can therefore be assumed to be related to the amounts of aligned and randomly oriented GO, respectively. If it is further assumed the aligned GO gives rise to the majority of the reinforcement in the system, then the parameter A can be used to estimate the effective Young's modulus of the aligned GO, again using the rule of mixtures. Inspection of the data in Table 1 shows that both A and the effective modulus decrease as the weight percent of GO is increased. If the parameter A represents the proportion of aligned GO in the sample, to a first approximation the Young's modulus of the aligned GO will be given by E_{eff}/A. The average value of E_{eff}/A calculated from the data in Table 1 is 210 ± 20 GPa, which is within the range of values of GO modulus determined from direct measurements[15,46] as described above.

The Raman band shift data give an independent estimate of the effective Young's modulus of the GO in the nanocomposites as shown in Table 2. The value determined in this present study is around 120 GPa and is similar to that derived from the mechanical data in Table 1 (as the wt% GO → 0). Figure 7 shows a schematic illustration of the factors that may lead to this discrepancy with the values determined from the direct measurements.[15,46] Figure 7a shows the situation for perfectly aligned GO flakes of finite length. In this case, the rule of mixtures should be obeyed with the strain in the GO being equal to the strain in the matrix. Because of the finite length of the flakes (≤10 μm) this will only be the case in the middle of

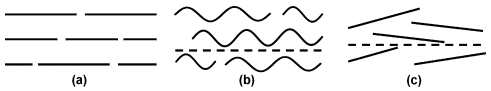

Figure 7. Illustrations of several possible alignments of GO in the PVA matrix: (a) perfect alignment, (b) wrinkles, (c) misorientation. The solid lines represent side views of GO flakes.

the flakes and the strain will decrease at the edges due to 'shear lag effects' as has been shown for monolayers of exfoliated graphene.[39] The magnitude of this effect will depend upon the strength of the GO-PVA interface, which although being probably stronger than in the case of graphene, at this stage is unknown. In any case it will lead to the effective modulus of the GO in the nanocomposites being lower than that measured directly. Another factor that will lead to a lower effective modulus of the GO is misalignment of the flakes either through waviness (Figure 7b) or off-axis alignment (Figure 7c). Using the analogy of off-axis fibres in a composite,[48] the axial strain in the flake will vary as $\cos^2\theta_x - \nu\sin^2\theta_x$, where is this case θ_x is the angle between the plane of the flake and the y-axis, and ν is the Poisson's ratio of the matrix. Any misorientation will lead to a proportionate reduction in the effective modulus of the GO determined either from the storage modulus or through Raman Band shifts. Aggregation of the GO will further reduce its effective modulus and its decrease with GO loading seen in Tables 1 and 2 may be a reflection of more aggregation occurring as the wt% GO increases.

CONCLUSIONS

A new insight has been obtained into the reinforcement of poly(vinyl alcohol) by graphene oxide through the use of Raman spectroscopy. It has been shown that there is a preferred orientation of GO flakes in the plane of the nanocomposite film and that it is possible to use polarized Raman spectroscopy to quantify the level of orientation. It has also been demonstrated that it is possible to follow stress transfer between the PVA matrix to the GO reinforcement from stress-induced shifts of the Raman D band. Moreover, it has been shown that it is possible to use the Grüneisen parameter to estimate the effective Young's modulus of the GO in the nanocomposites from the rate of shift of the D band per unit strain to be around 120 GPa. It is further shown that the effective modulus determined by this method is similar to that obtained using the measured storage modulus and the simple rule of mixtures. In both cases the effective Young's modulus of the GO is found to decrease as the weight percent of GO increases and this has been shown to be consistent with a decrease in the degree of alignment of the GO with increasing loading determined using polarized Raman spectroscopy and aggregation effects. It is clear that the technique of using the Raman D-band to follow the deformation of graphene oxide in nanocomposites that has been developed in this study will have important implications in the future for the analysis graphene oxide-based nanocomposites.

ASSOCIATED CONTENT

Supporting Information

Further experimental data are given upon the characterization of the GO and GO/PVA nanocomposites using SEM, AFM, XRD, and polarized Raman spectroscopy. The shift in the D band with strain for different GO loadings is also shown. This material is available free of charge via the Internet at http://pubs.acs.org.

AUTHOR INFORMATION

Corresponding Author

*E-mail: robert.young@manchester.ac.uk.

Notes

The authors declare no competing financial interest.

ACKNOWLEDGMENTS

The authors are grateful for support from the EPSRC, China Scholarship Council (Z.L.), and AFOSR/EOARD (Award FA8655-12-1-2058).

REFERENCES

(1) Novoselov, K. S.; Geim, A. K.; Morozov, S. V.; Jiang, D.; Zhang, Y.; Dubonos, S. V.; Grigorieva, I. V.; Firsov, A. A. *Science* **2004**, *306*, 666−669.
(2) Liang, J. J.; Xu, Y. F.; Huang, Y.; Zhang, L.; Wang, Y.; Ma, Y. F.; Li, F. F.; Guo, T. Y.; Chen, Y. S. *J. Phys. Chem. C* **2009**, *113*, 9921−9927.
(3) Liang, J. J.; Huang, L.; Li, N.; Huang, Y.; Wu, Y. P.; Fang, S. L.; Oh, J. Y.; Kozlov, M.; Ma, Y. F.; Li, F. F.; Baughman, R.; Chen., Y. S. *ACS Nano* **2012**, *6*, 4508−4519.
(4) Stankovich, S.; Dikin, D. A.; Dommett, G. H. B.; Kohlhaas, K. M.; Zimney, E. J.; Stach, E. A.; Piner, R. D.; Nguyen, S. T.; Ruoff, R. S. *Nature* **2006**, *442*, 282−286.
(5) Kim, H.; Abdala, A. A.; Macosko, C. W. *Macromolecules* **2010**, *43*, 6515−6530.
(6) Young, R. J.; Kinloch, I. A.; Gong, L.; Novoselov, K. S. *Compos. Sci. Technol.* **2012**, *72*, 1459−1476.
(7) Dikin, D. A.; Stankovich, S.; Zimney, E. J.; Piner, R. D.; Dommett, G. H. B.; Evmenenko, G.; Nguyen, S. T.; Ruoff, R. S. *Nature* **2007**, *448*, 457−460.
(8) He, H. Y.; Klinowski, J.; Forster, M.; Lerf, A. *Chem. Phys. Lett.* **1998**, *287*, 53−56.
(9) Wilson, N. R.; Pandey, P. A.; Beanland, R.; Young, R. J.; Kinloch, I. A.; Gong, L.; Liu, Z.; Suenaga, K.; Rourke, J. P.; York, S. J.; Sloan, J. *ACS Nano* **2009**, *3*, 2547−2556.
(10) Rourke, J. P.; Pandey, P. A.; Moore, J. J.; Bates, M.; Kinloch, I. A.; Young, R. J.; Wilson, N. R. *Angew. Chem., Int. Ed.* **2011**, *50*, 3173−3177.
(11) Xu, Y.; Hong, W.; Bai, H.; Li, C.; Shi, G. *Carbon* **2009**, *47*, 3538−3543.
(12) Liang, J.; Huang, Y.; Zhang, L.; Wang, Y.; Ma, Y.; Guo, T.; Chen, Y. *Adv. Funct. Mater.* **2009**, *19*, 2297−2302.
(13) Putz, K. W.; Compton, O. C.; Palmeri, M. J.; Nguyen, S. T.; Brinson, L. C. *Adv. Funct. Mater.* **2010**, *20*, 3322−3329.
(14) Zhao, X.; Zhang, Q. H.; Chen, D. J.; Lu, P. *Macromolecules* **2010**, *43*, 2357−2363.
(15) Suk, J. W.; Piner, R. D.; An, J.; Ruoff, R. S. *ACS Nano* **2010**, *4*, 6557−6564.
(16) Bao, C.; Guo, Y.; Song, L.; Hu, Y. *J. Mater. Chem.* **2011**, *21*, 13942−13950.
(17) Cronin, S. B.; Swan, A. K.; Ünlü, M. S.; Goldberg, B. B.; Dresselhaus, M. S.; Tinkham, M. *Phys. Rev. Lett.* **2004**, *93*, 167401.
(18) Mohiuddin, T. M. G.; Lombardo, A.; Nair, R. R.; Bonetti, A.; Savini, G.; Jalil, R.; Bonini, N.; Basko, D. M.; Galiotis, C.; Marzari, N.; Novoselov, K. S.; Geim, A. K.; Ferrari, A. C. *Phys. Rev. B* **2009**, *79*, 205433.
(19) Huang, M.; Yan, H.; Chen, C.; Song, D.; Heinz, T. F.; Hone, J. *Proc. Natl. Acad. Sci. U.S.A.* **2009**, *106*, 7304−7308.
(20) Robinson, I. M.; Zakikhani, M.; Day, R. J.; Young, R. J.; Galiotis, C. *J. Mater. Sci. Lett.* **1987**, *6*, 1212−1214.
(21) Cooper, C. A.; Young, R. J.; Halsall, M. *Compos. A: Appl. Sci. Manu.* **2001**, *32*, 401−411.
(22) Young, R. J.; Gong, L.; Kinloch, I. A.; Riaz, I.; Jalil, R.; Novoselov, K. S. *ACS Nano* **2011**, *5*, 3079−3084.
(23) Yang, D.; Velamakanni, A.; Bozoklu, G.; Park, S.; Stoller, M.; Piner, R. D.; Stankovich, S.; Jung, I.; Field, D. A.; Ventrice, C. A., Jr; Ruoff, R. S. *Carbon* **2009**, *47*, 145−152.
(24) Gao, Y.; Liu, L.-Q.; Zu, S.-Z.; Peng, K.; Zhou, D.; Han, B.-H.; Zhang, Z. *ACS Nano* **2011**, *5*, 2134−2141.
(25) Hummers, W. S.; Offeman, R. E. *J. Am. Chem. Soc.* **1958**, *80*, 1339−1339.
(26) Xu, Y.; Sheng, K.; Li, C.; Shi, G. *ACS Nano* **2010**, *4*, 4324−4330.

(27) Salavagione, H. J.; Martinez, G.; Gomez, M. A. *J. Mater. Chem.* **2009**, *19*, 5027−5032.
(28) Deng, L.; Eichhorn, S. J.; Kao, C.-C.; Young, R. J. *ACS Appl. Mater. Interfaces* **2011**, *3*, 433−440.
(29) Yang, X.; Li, L.; Shang, S.; Tao, X.-M. *Polymer* **2010**, *51*, 3431−3435.
(30) Kim, H. M.; Lee, J. K.; Lee, H. S. *Thin Solid Films* **2011**, *519*, 7766−7771.
(31) Zabel, J.; Nair, R. R.; Ott, A.; Georgiou, T.; Geim, A. K.; Novoselov, K. S.; Casiraghi, C. *Nano Lett.* **2011**, *12*, 617−621.
(32) Ferrari, A. C.; Robertson, J. *Phys. Rev. B* **2000**, *61*, 14095−14107.
(33) Kudin, K. N.; Ozbas, B.; Schniepp, H. C.; Prud'homme, R. K.; Aksay, I. A.; Car, R. *Nano Lett.* **2007**, *8*, 36−41.
(34) Ferrari, A. C.; Meyer, J. C.; Scardaci, V.; Casiraghi, C.; Lazzeri, M.; Mauri, F.; Piscanec, S.; Jiang, D.; Novoselov, K. S.; Roth, S.; Geim, A. K. *Phys. Rev. Lett.* **2006**, *97*, 187401.
(35) López-Honorato, E.; Meadows, P. J.; Shatwell, R. A.; Xiao, P. *Carbon* **2010**, *48*, 881−890.
(36) Gommens, H. H.; Alldredge, J. W.; Tashiro, H.; Park, J.; Magnuson, J.; Rinzler, A. G. *J. Appl. Phys.* **2000**, *88*, 2509−2514.
(37) Liang, Q. Z.; Yao, X. X.; Wang, W.; Liu, Y.; Wong, C. P. *ACS Nano* **2011**, *5*, 2392−2401.
(38) Young, R. J.; Lovell, P. A. *Introduction to Polymers*, 3rd ed.; CRC Press: London, 2011; Chapter 24.
(39) Gong, L.; Kinloch, I. A.; Young, R. J.; Riaz, I.; Jalil, R.; Novoselov, K. S. *Adv. Mater.* **2010**, *22*, 2694−2697.
(40) Gong, L.; Young, R. J.; Kinloch, I. A.; Riaz, I.; Jalil, R.; Novoselov, K. S. *ACS Nano* **2012**, *6*, 2086−2095.
(41) Frank, O.; Tsoukleri, G.; Riaz, I.; Papagelis, K.; Parthenios, J.; Ferrari, A. C.; Geim, A. K.; Novoselov, K. S.; Galiotis, C. *Nat. Commun.* **2011**, *2*, 255.
(42) Grimvall, G. Phonons in Real Crystals: Anharmonic Effects. In *Thermophysical Properties of Materials*; Elsevier Science B.V.: Amsterdam, 1999; Chapter 8, pp 136−152.
(43) Ferralis, N. *J. Mater. Sci.* **2010**, *45*, 5135−5149.
(44) Ding, F.; Ji, H.; Chen, Y.; Herklotz, A.; Dörr, K.; Mei, Y.; Rastelli, A.; Schmidt, O. G. *Nano Lett.* **2010**, *10*, 3453−3458.
(45) Lee, C.; Wei, X. D.; Kysar, J. W.; Hone, J. *Science* **2008**, *321*, 385−388.
(46) Gomez-Navarro, C.; Burghard, M.; Kern, K. *Nano Lett.* **2008**, *8*, 2045−2049.
(47) Paci, J. T.; Belytschko, T.; Schatz, G. C. *J. Phys. Chem. C* **2007**, *111*, 18099−18111.
(48) Andrews, M. C.; Day, R. J.; Hu, X.; Young, R. J. *J Mater. Sci. Lett.* **1992**, *11*, 1344−1346.